Fast characterization of two ultrasound longitudinal waves in cancellous bone using an adaptive beamforming technique

Hirofumi Taki[a)]
Graduate School of Engineering, Tohoku University, Sendai 980-8579, Japan

Yoshiki Nagatani
Department of Electronics, Kobe City College of Technology, Kobe 651-2194, Japan

Mami Matsukawa
Faculty of Science and Engineering, Doshisha University, Kyotanabe 610-0321, Japan

Katsunori Mizuno
Institute of Industrial Science, The University of Tokyo, Tokyo 113-8654, Japan

Toru Sato
Graduate School of Informatics, Kyoto University, Kyoto 606-8501, Japan

(Received 6 September 2014; revised 18 January 2015; accepted 4 March 2015)

The received signal in through-transmission ultrasound measurements of cancellous bone consists of two longitudinal waves, called the fast and slow waves. Analysis of these fast and slow waves may reveal characteristics of the cancellous bone that would be good indicators of osteoporosis. Because the two waves often overlap, decomposition of the received signal is an important problem in the characterization of bone quality. This study proposes a fast and accurate decomposition method based on the frequency domain interferometry imaging method with a modified wave transfer function that uses a phase rotation parameter. The proposed method accurately characterized the fast and slow waves in the experimental study, and the residual intensity, which was normalized with respect to the received signal intensity, was less than −20 dB over the bone specimen thickness range from 6 to 15 mm. In the simulation study, the residual intensity was less than −20 dB over the specimen thickness range from 3 to 8 mm. Decomposition of a single received signal takes only 5 s using a laptop personal computer with a single central processing unit. The proposed method has great potential to provide accurate and rapid measurements of indicators of osteoporosis in cancellous bone.
 [http://dx.doi.org/10.1121/1.4916276]

[GH] Pages: 1683–1692

I. INTRODUCTION

Osteoporosis is a disease that is characterized by a decrease in bone mass, leading to an increased possibility of the risk of bone fracture. Dual x-ray absorptiometry is the gold standard for osteoporosis diagnosis; however, diagnosis using this method is based on only one parameter related to bone porosity (Genant and Jiang, 2006; Blake and Fogelman, 2007). Additional testing using another modality may improve the accuracy of the diagnosis of osteoporosis.

Quantitative ultrasound (QUS) is one technique that offers the potential to estimate the possibility of osteoporosis without using ionizing radiation (Langton *et al.*, 1984; Laugier, 2008; Barkmann *et al.*, 2008a,b). QUS measures the speed of sound and the broadband ultrasonic attenuation characteristics that provide important information for characterization of bone quality and strength (Bouxsein *et al.*, 1995; Njeh *et al.*, 1997; Han *et al.*, 1997; Lochmüller *et al.*, 1999; Haïat *et al.*, 2009). It has been established that the received signal in through-transmission ultrasound measurements of cancellous bone consists of the fast and slow waves (Hosokawa and Otani, 1997, 1998; Hughes *et al.*, 1999; Kaczmarek *et al.*, 2002; Cardoso *et al.*, 2003; Fellah *et al.*, 2004). Several studies have reported that analysis of these fast and slow waves may reveal the characteristics of cancellous bone (Cardoso *et al.*, 2003; Haïat *et al.*, 2007; Hughes *et al.*, 2007; Hosokawa, 2009; Mizuno *et al.*, 2008; Mizuno *et al.*, 2009). Because the characteristics of cancellous bone provide good indications of the bone changes caused by osteoporosis (Njeh *et al.*, 1999), fast and accurate characterization of the fast and slow waves may be important to the realization of an osteoporosis screening method.

Analysis of the fast and slow waves requires decomposition of the received signal from cancellous bone into the fast and slow waves. Because the two waves often overlap, decomposition of the received signal is an important problem in the characterization of bone quality using QUS. One proposed strategy is the application of a Bayesian method using a Markov chain Monte Carlo method with simulated annealing (Marutyan *et al.*, 2007; Anderson *et al.*, 2010; Nelson *et al.*, 2011; Hoffman *et al.*, 2012). The Bayesian decomposition method succeeded in accurately characterizing the fast and slow waves of a received signal from cancellous bone; however, this method involves a considerable computational load.

Other groups have reported fast decomposition methods for characterization of the fast and slow waves. The space-alternating generalized expectation-maximization method

[a)]Author to whom correspondence should be addressed. Electronic mail: taki@ecei.tohoku.ac.jp

has been applied to signals that simulated the received signal from a proximal femur (Dencks and Schmitz, 2013). Wear reported that both the modified least squares Prony's method with curve fitting (Wear, 2013) and band-limited deconvolution (Wear, 2014) are suitable for rapid characterization of the fast and slow waves. However, these fast decomposition methods have only modest accuracy when compared with that of the Bayesian decomposition method.

In the present study, we propose a fast decomposition method based on frequency domain interferometry (FDI), with decomposition accuracy that is similar to that of a Bayesian method. We explain the methodology of the proposed decomposition method, present experimental results, and offer discussion and conclusions related to our findings.

II. METHODS

The proposed decomposition method requires no prior information about the characteristics of a bone specimen, e.g., the specimen thickness. The method uses a specific parameter set for the bone characteristics, and estimates the specimen thickness as part of the decomposition process. After decomposition, we can estimate the characteristics of the bone specimen using its true thickness and the estimated thickness. In this section, we explain the modified transfer functions used for the fast and slow waves that satisfy the Kramers–Kronig relations. We then describe the proposed decomposition method based on the FDI imaging method.

A. Transfer functions for fast and slow waves

The wave propagation in cancellous bone has been modeled in previous studies (Marutyan *et al.*, 2006; Anderson *et al.*, 2008). The conventional propagation models are expressed using the following formula:

$$S_{\mathrm{R}}(f) = S_{\mathrm{I}}(f)[H_1(f) + H_2(f)], \tag{1}$$

where $S_{\mathrm{R}}(f)$ is a frequency component of the received signal passing through a bone specimen in water at frequency f, $S_{\mathrm{I}}(f)$ is the same component passing through a water-only path, and $H_1(f)$ and $H_2(f)$ are the transfer functions for the fast and slow waves, respectively. Several researchers have used a transfer model that assumes that the fast and slow waves are propagating simultaneously through a medium exhibiting linear-with-frequency attenuation (Nelson *et al.*, 2011; Wear, 2013, 2014). This model introduces the assumption that the wavefront of an ultrasound wave passing through a bone specimen in water is the same as that passing through a water-only path. However, the heterogeneity of cancellous bone causes complicated changes in the wavefronts as they pass. Because the ultrasound waves are typically received by a flat transducer, an uneven wavefront has an effect on the transfer function. In this study, we approximate this effect using the following formula:

$$s_{\mathrm{R}}{}'(t) = \int [f_{\mathrm{T1}}(\tau)s_{\mathrm{R1}}(t-\tau) + f_{\mathrm{T2}}(\tau)s_{\mathrm{R2}}(t-\tau)]d\tau, \tag{2}$$

where $s_{\mathrm{R}}{}'(t)$ is the received signal of the proposed model in the time domain, $s_{\mathrm{R1}}(t)$ and $s_{\mathrm{R2}}(t)$ are the fast and slow wave signals of the conventional model in the time domain, respectively, and $f_{\mathrm{T1}}(t)$ and $f_{\mathrm{T2}}(t)$ are the functions that express the arrival time distributions of the wavefront at the receive element for the fast and slow waves, respectively. The frequency component of the received signal in the proposed method is expressed as

$$S_{\mathrm{R}}{}'(f) = \mathbf{F}[s_{\mathrm{R}}{}'(t)] = S_{\mathrm{I}}(f)[F_{\mathrm{T1}}(f)H_1(f) + F_{\mathrm{T2}}(f)H_2(f)], \tag{3}$$

where $\mathbf{F}$ denotes a Fourier transform, and $F_{\mathrm{T1}}(f)$ and $F_{\mathrm{T2}}(f)$ are the frequency components of the arrival time distributions of the fast and slow waves, respectively. We call this effect, which is caused by the arrival time distribution of the wavefront, the path-length-variation (PLV) effect.

Figure 1 shows an example of the arrival time distribution of the wavefront at the receive element, and of the PLV effect on the intensity and phase in the frequency domain. In this case, the distribution follows a chi-squared distribution with three degrees of freedom. Typically, the phase of $F_{\mathrm{T}i}(f)$ is not proportional to f and the intensity of $F_{\mathrm{T}i}(f)$ is not constant, where $i = 1$ and 2 for the fast and slow waves, respectively. Therefore, we approximate $F_{\mathrm{T}i}(f)$ in the main frequency band using the following formula:

$$F_{\mathrm{T}i}(f) \cong A_{\mathrm{T}i} \exp[-\gamma_i f + j(\delta_i f + \theta_i)], \tag{4}$$

where $A_{\mathrm{T}i}$, γ_i, σ_i, and θ_i are real constants. $\gamma_i f$ and $j\sigma_i f$ denote the attenuation and the time shift caused by the arrival time distribution at the receive element, respectively. We call θ_i the phase rotation parameter, and it is independent of f. The modified transfer function with the additional phase rotation parameter is expressed by the following formula:

$$\begin{aligned} H_i{}'(f) &= F_{\mathrm{T}i}(f)H_i(f) \\ &= A_i{}' \exp\left[-\beta_i{}' f d + j\left\{\frac{2\pi f d}{c_i(f)} - \frac{2\pi f d}{c_{\mathrm{W}}}\right\} + j\delta_i f + j\theta_i\right], \end{aligned} \tag{5}$$

$$A_i{}' = A_i A_{\mathrm{T}i}, \tag{6}$$

$$\beta_i{}' = \beta_i + \frac{\gamma_i}{d}, \tag{7}$$

where A_i is the signal amplitude parameter that is independent of f, β_i is the slope of attenuation, i.e., broadband ultrasonic attenuation parameter, in the conventional model, d is the bone specimen thickness, $c_i(f)$ is the phase velocity, and c_{W} is the sound velocity in water. $A_i{}'$ and $\beta_i{}'$ are real constants, and $j\delta_i f$ denotes the time shift. Therefore, the major modification made in the proposed model is the introduction of the phase rotation parameter θ_i. The introduction of this parameter compensates for the waveform change caused by the uneven wavefront.

In this study, we assume that c_{W} has a constant value. When the medium has linear-with-frequency attenuation, the phase velocities of the fast and slow waves can be expressed by the following formula (Waters *et al.*, 2005):

$$\frac{1}{c_i(f)} - \frac{1}{c_i(f_0)} = -\frac{\beta_i}{\pi^2} \ln\left(\frac{f}{f_0}\right), \tag{8}$$

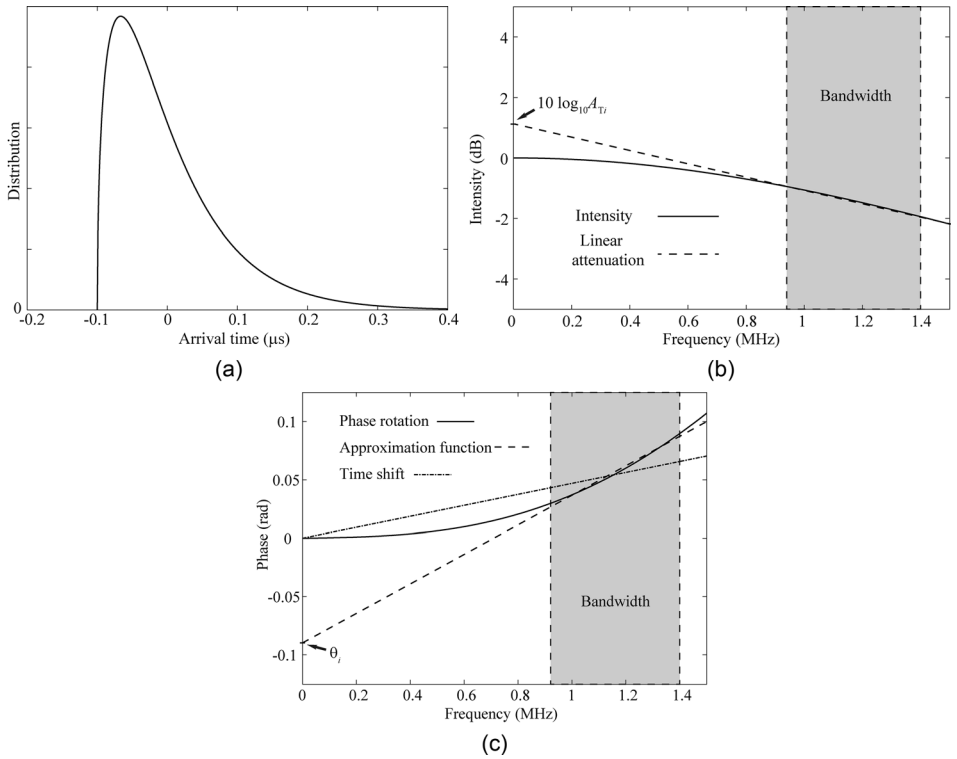

FIG. 1. (a) Example of the arrival time distribution of the wavefront at the receive element, and (b) its intensity and (c) phase in the frequency domain. In this case, the distribution follows a chi-squared distribution with three degrees of freedom. We employ linear-with-frequency models to approximate the effect of the arrival-time-distribution on the intensity and phase rotation in the major frequency band. A_{Ti} and θ_i are the intensity and phase rotation parameters given in Eq. (4), respectively.

where f_0 is a reference frequency.

We applied the proposed method to simulated and experimental data measured in a previous work (Nagatani *et al.*, 2008). To prepare $S_I(f)$, we used the received signal passing through water in an acoustic tube, where the center frequency of the pulse was 1 MHz and the pulse length was equal to one wavelength at the center frequency. Planar polyvinylidene fluoride transducers were used for both transmitter and receiver. In this experiment, the bone specimen was immersed in water in the acoustic tube. In the simulation study, the bone specimen size was $17 \times 17 \times d$ mm, where the bone specimen thickness d varied from 2 to 9 mm. In the experimental study, the bone specimen size was $20 \times 20 \times d$ mm, where the bone specimen thickness d varied from 6 to 15 mm.

The proposed decomposition method used propagation parameters that were reported in a previous study (Nelson *et al.*, 2011) as the provisional parameter set. This study also used the experimental data reported by Nagatani *et al.* (2008), and the parameters were estimated by application of a Bayesian decomposition method to the received signal for a bone specimen thickness of 9 mm. This setting modifies the transfer function given by Eq. (5) to become

$$H_i'(f) \cong A_i' \exp\left[-\beta_{Pi} f d_{Ti} + j\left\{ \frac{2\pi f d_{Ti}}{c_{Pi}(f)} - \frac{2\pi f d_{Ti}}{c_W} \right\} + j\delta_i' f + j\theta_i' \right], \tag{9}$$

$$\frac{1}{c_{Pi}(f)} - \frac{1}{c_i(f_0)} = -\frac{\beta_{Pi}}{\pi^2} \ln\left(\frac{f}{f_0}\right), \tag{10}$$

where d_{Ti} is the temporal specimen thickness, and $\beta_{Pi} f$ and $c_{Pi}(f)$ denote the provisional attenuation coefficient and the phase velocity that were reported in Nelson *et al.* (2011), respectively. In this study, β_{P1} and β_{P2} were 49.2 and 7.1 dB/cm/MHz, respectively, f_0 was 1 MHz, and $c_{P1}(f_0)$ and $c_{P2}(f_0)$ were 1933 and 1475 m/s, respectively. The proposed decomposition method does not require A_1 and A_2, because it estimated the parameters in a decomposition process. The temporal specimen thickness d_{Ti} is never the same as the estimated thickness, as emphasized in this study, because the optimum value of d_{Ti} satisfies the equation $\beta_{Pi} d_{Ti} = \beta_i' d$. That is, the use of d_{Ti} can compensate for the difference between the optimum attenuation $\beta_i' f$ and the provisional attenuation $\beta_{Pi} f$. Therefore, the modification of Eq. (9) assumes application of the formula expressed by

$$\frac{2\pi f d_{Ti}}{c_{Pi}(f)} - \frac{2\pi f d}{c_i(f)} - \frac{2\pi f (d_{Ti} - d)}{c_W} \cong \delta_i'' f + \theta_i'', \tag{11}$$

where δ_i'' and θ_i'' are real constants. When the assumption given by Eq. (11) is valid, the application of a time shift and a phase rotation to the conventional model can produce appropriate fast and slow waves. The proposed method optimizes four parameters; the signal amplitude parameter A_i', the temporal specimen thickness d_{Ti}, the time shift parameter δ_i', and the phase rotation θ_i'.

Figure 2 shows the waveforms of the fast and slow waves that were calculated using the modified transfer function in the experimental study, where the specimen thickness varied from 5 to 25 mm and the phase rotation parameter was 0°. The envelope amplitude of each wave was normalized, and the rise time of each wave was set to $t = 0$ s after a time shift process. In this study, we defined the rise time of each wave as the time when the normalized amplitude first exceeds 0.01, where specimen thicknesses are 5 and 20 mm. The rise times for other thicknesses were determined by interpolation and extrapolation. As shown in Fig. 2, the rise

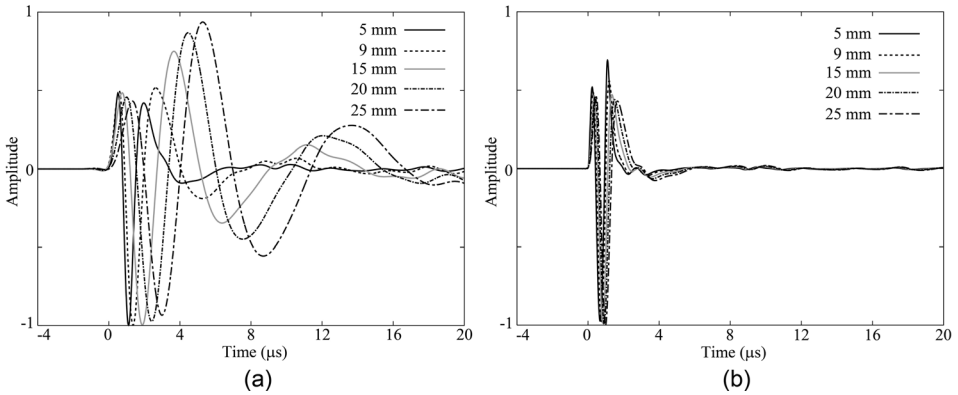

FIG. 2. Waveforms of (a) fast and (b) slow waves calculated using the modified transfer function in the experimental study. The specimen thickness d ranges from 5 to 25 mm. The phase rotation parameter θ_i is 0°.

times of the fast and slow waves were determined stably. We can use another process to determine the rise time of each wave. The phase rotation parameter θ_i changes the waveforms of the fast and slow waves, as shown in Fig. 3.

B. Deconvolution method based on the FDI imaging method

The proposed deconvolution method consists of two parts; the first is the initial estimation of the fast and slow waves using the FDI imaging method, and the second is the conclusive estimation using the least squares method in the time domain. Figure 4 shows a flowchart for the proposed deconvolution method.

1. Initial estimation using the FDI imaging method

Typically, the amplitude of the fast wave is lower than that of the slow wave. Because the fast wave is received earlier than the slow wave, the proposed method selects a time window for estimation of a fast wave, where the response of the slow wave is negligible within that time window. To select a time threshold that separates the fast and slow waves, a previous work used a local minimum in the envelope of the received signal in the time domain (Wear, 2014). However, it is difficult to use this strategy under the strict condition that the peak amplitude position of the fast wave is located close to the fast wave in the time domain. The first purpose of using the FDI imaging method is for accurate selection of the rise time of the slow wave, T_S. The second purpose is to prepare candidate waves for the fast and slow waves.

The FDI imaging method is a high-range-resolution imaging method that uses an adaptive beamforming technique (Taki *et al.*, 2012). The method suppresses the contributions of undesired echoes under the constraint that a reference signal must give a constant response. Therefore, we construct several candidate waves for the fast and slow waves using the modified transfer function that was described in Sec. II A, where each candidate is used as the reference signal in the FDI imaging method. The estimated intensity calculated by the FDI imaging method is normalized with respect to the amplitude of the employed reference signal. To eliminate the effect of this normalization on the estimated intensity, we set the peak amplitude of each envelope to 1.

The FDI imaging method was designed based on the condition that a narrowband signal is used, and it assumes that all frequency components of a single wave have the same intensity and phase. During the application of ultrasound using a broadband signal, the intensity and the phase of a frequency component of a single wave vary with the frequency. To ensure that the intensity and phase of the frequency components are uniform, each frequency component of a received signal is normalized with respect to the reference signal (Taki *et al.*, 2012),

$$X_{\mathrm{H}l} = X_l X_{\mathrm{R}l}^{*} / (|X_{\mathrm{R}l}|^2 + \eta), \tag{12}$$

where X_l, $X_{\mathrm{H}l}$, and $X_{\mathrm{R}l}$ are the lth frequency components of the received signal, of the received signal after normalization, and of the reference signal, respectively, the superscript asterisk denotes the complex conjugate, and η is a constant term used for stabilization. In this study, we set the value of

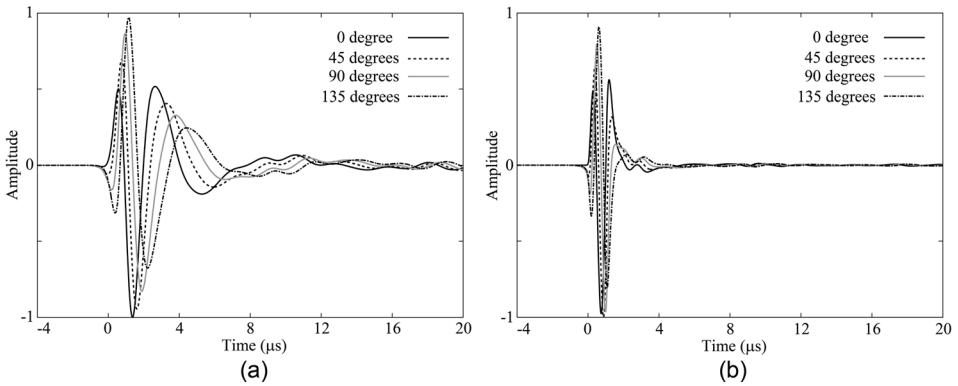

FIG. 3. Waveforms of (a) fast and (b) slow waves calculated using the modified transfer function in the experimental study. The specimen thickness d is 9 mm. The phase rotation parameters θ_i are 0°, 45°, 90°, and 135°.

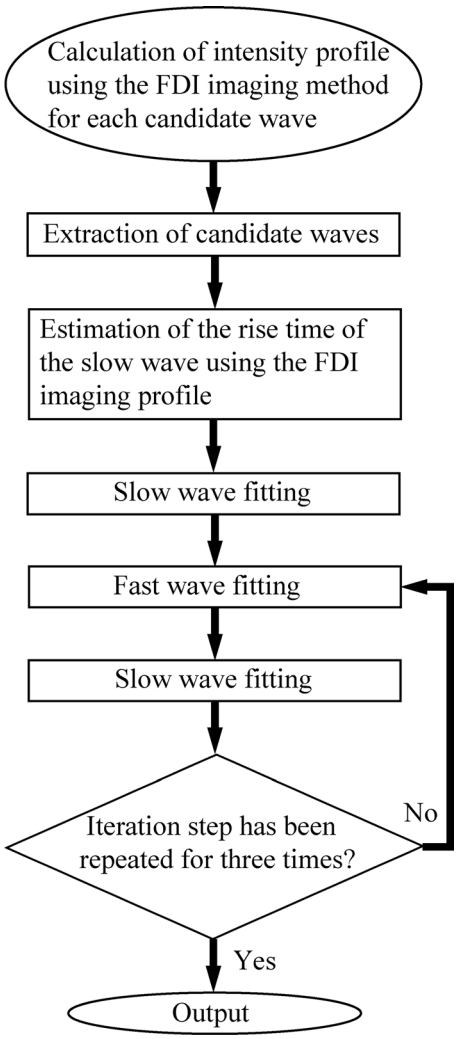

FIG. 4. Flowchart of the proposed deconvolution method.

η to be 40 dB lower than the average intensity of the reference signal, $X_{\mathrm{R}l}$.

The phase of each frequency component of a received signal $X_{\mathrm{H}l}$ depends on the product of its frequency and the path length. The output intensity of the FDI imaging method is therefore formulated as follows:

$$P(r) = |\mathbf{X}_{\mathrm{H}}^{\mathrm{T}}\mathbf{W}^{*}|^{2} = \mathbf{W}^{\mathrm{T}*}\mathbf{R}\mathbf{W}, \tag{13}$$

$$\mathbf{R} = \mathbf{X}_{\mathrm{H}}\mathbf{X}_{\mathrm{H}}^{\mathrm{T}*}, \tag{14}$$

where $r/2$ is the measurement depth, $\mathbf{X}_{\mathrm{H}}$ is the received signal vector that consists of $X_{\mathrm{H}l}$, the superscript T denotes the transpose, and $\mathbf{W}$ is a weighting vector used for phase compensation. The simplest setting is the employment of a fixed weighting vector given by

$$\mathbf{W} = [\, e^{jk_1 r} \quad e^{jk_2 r} \quad \cdots \,]^{\mathrm{T}}, \tag{15}$$

where k_l is the lth wavenumber of the frequency components.

The proposed FDI imaging method uses the Capon method, which is an adaptive beamforming technique. However, the FDI imaging method using the Capon method does not work when the waves are correlated with each other. Therefore, we must suppress the correlation between the fast and slow waves. The employment of the frequency averaging technique suppresses the correlation between the two waves (Taki *et al.*, 2012),

$$\mathbf{R}_{\mathrm{A}} = \frac{1}{M}\sum_{m=1}^{M}\mathbf{R}_m, \tag{16}$$

where $\mathbf{R}_{\mathrm{A}}$ is the covariance matrix after frequency averaging, M is the number of sub-matrices used for frequency averaging, and $\mathbf{R}_m$ is a sub-matrix of $\mathbf{R}$ where the (i', j') element of $\mathbf{R}_m$ corresponds to the $(i'+m-1, j'+m-1)$ element of $\mathbf{R}$.

The FDI imaging method with the Capon method suppresses any undesired echoes under the constraint of a constant response for the reference signal at a measurement depth (Capon, 1969). This problem is expressed by the following formulas:

$$\min \quad \mathbf{W}^{\mathrm{T}*}\mathbf{R}_{\mathrm{A}}\mathbf{W} \quad \text{subject to} \quad \mathbf{C}^{\mathrm{T}*}\mathbf{W} = 1\,, \tag{17}$$

$$\mathbf{C} = [\, e^{jk_1 r} \quad e^{jk_2 r} \quad \cdots \quad e^{jk_L r} \,]^{\mathrm{T}}, \tag{18}$$

where L is the size of $\mathbf{R}_{\mathrm{A}}$. This problem can be solved by the application of Lagrange multiplier methods without the iteration process, as emphasized in this study (Taki *et al.*, 2012). When the optimum weighting vector is used, the estimated intensity can be expressed using the following formulas:

$$P_{\mathrm{Cap}}(r) = \frac{1}{\mathbf{C}^{\mathrm{T}*}(\mathbf{R}_{\mathrm{A}} + \eta'\mathbf{E})^{-1}\mathbf{C}}, \tag{19}$$

where $\eta'\mathbf{E}$ is a diagonal loading used for stabilization. In this study, we set the value of η' to be 40 dB lower than the average of the diagonal elements of $\mathbf{R}_{\mathrm{A}}$. Equation (19) indicates that only a single calculation of the inverse matrix is required to acquire the estimated intensity profile for all depths without calculation of the optimum weighting vector. The FDI imaging method is therefore suitable for real-time signal processing applications.

When the waveform of a candidate is unlike that of the slow wave, the output intensity estimated by the FDI imaging method generally decreases. In other words, the output intensity will be at a maximum when the candidate waveform is closest to the waveform of the slow wave. We therefore calculate the intensity profiles of all candidates for the slow waves, and select the candidate where the peak intensity in its profile is the highest among all candidates. We use the depth of the peak intensity of the selected candidate for the rise time of the slow wave. In the least mean squares process, we extracted the candidates with peak intensities that were higher than 1/100 of the maximum peak intensity. In the FDI imaging process, we prepared 11 candidates for each of the fast and slow waves, where the thickness d ranged from 5 to 25 mm and the sampling interval is 2 mm. In the fast wave case, the rise time and the candidate extraction for the least squares method were determined by the same process that was used for the slow wave, with the

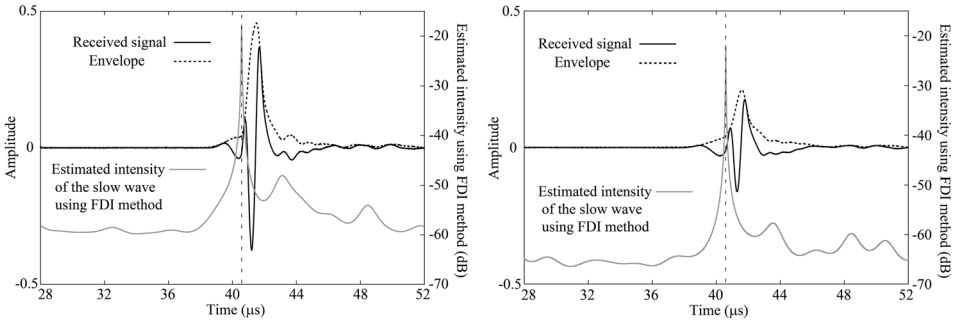

FIG. 5. Slow wave intensity estimated using the FDI imaging method when the specimen thickness is (a) 9 mm and (b) 12 mm in the experimental study. The vertical broken line corresponds to the rise time of the slow wave as estimated by the FDI imaging method.

exception that the rise time of the fast wave should be at least 0.4 μs earlier than that of the slow wave.

Figure 5 shows the intensity profile of the slow wave that was estimated using the FDI imaging method in the experimental study. Wear used the local minimum of the envelope to determine the border between the fast and slow waves (Wear, 2014). However, in many cases, no local minimum exists for the envelope, as shown in Fig. 5. In contrast, the estimated intensity profile of the slow wave that was calculated by the FDI imaging method shows a sharp peak at the rise time of the slow wave, T_S. Therefore, the FDI imaging method is suitable for determination of the border between the fast and slow waves.

2. Conclusive estimation using the least squares method

The proposed decomposition method uses the least squares method in the time domain to characterize the fast and slow waves. In the characterization process, the proposed method optimizes the signal amplitude parameter A_i', the temporal specimen thickness d_{Ti}, the rise time $T_{Ri} = -\delta_i'/2\pi$, and the phase rotation θ_i', as expressed in Eq. (9). When $T_{Ri} = 0$, i.e., $\delta_i' = 0$, a candidate for the fast and slow waves in the time domain is expressed using the following formulas:

$$\begin{aligned} s_i(d_{Ti}, A_i', \theta_i', t) &= \mathrm{Re}\{\mathbf{F}^{-1}[S_I(f)H_i'(f)_{\delta_i'=0}]\} \\ &\cong A_i' \cos\theta_i' \mathrm{Re}\{s_i'(t)\} \\ &\quad + A_i' \sin\theta_i' \mathrm{Re}\{j s_i'(t)\}, \end{aligned} \tag{20}$$

$$s_i'(t) = \mathbf{F}^{-1}\left(S_I(f)\exp\left[-\beta_{Pi} f d_{Ti} + j\left\{\frac{2\pi f d_{Ti}}{c_{Pi}(f)} - \frac{2\pi f d_{Ti}}{c_W}\right\}\right]\right), \tag{21}$$

where $\mathbf{F}^{-1}$ denotes an inverse Fourier transform. Estimation of the fast and slow waves uses minimization of the sum of squares D on four variables,

$$D(d_{Ti}, A_i', \theta_i', T_{Ri}) = \sum_{t=T_1}^{T_2} |s_o(t) - s_i(d_{Ti}, A_i', \theta_i', t - T_{Ri})|^2, \tag{22}$$

where $s_o(t)$ is the objective function used for fitting, and $T_1 \le t \le T_2$ is a fitting region. The proposed method uses provisional constant values for β_{Pi} and c_{Pi}, and the waveform of $s_i'(t)$ varies with the single variable d_{Ti}. Because each value of $A_i'\cos\theta_i'$ and $A_i'\sin\theta_i'$ is a real number, estimation of A_i' and θ_i' requires a single linear least squares process on two variables for each variable set of d_{Ti} and T_{Ri}. Therefore, the number of linear least squares processes required is the product of the number of specimen thickness candidates d_{Ti} and the number of rise time candidates T_{Ri}.

In the least mean squares process, we prepared 111 candidates for each of the fast and slow waves, where d ranged from 4 to 26 mm and the sampling interval was 0.2 mm. Because candidate extraction using the FDI imaging method reduced the number of candidates, the number of candidates that was actually used in the least mean squares process was 111 or less. The rise time candidates ranged from $T_{i\mathrm{FDI}} - 0.8\,\mu$s to $T_{i\mathrm{FDI}} + 0.8\,\mu$s, where $T_{i\mathrm{FDI}}$ is the rise time calculated using the FDI imaging method, and $T_{2\mathrm{FDI}} = T_S$.

For characterization of the fast and slow waves, we selected the fitting region $T_A \le t \le T_P$, as shown in Fig. 6. In this study, $T_A = T_E - 4\,\mu$s and $T_P = T_E + 0.8\,\mu$s, where T_E is the peak time of the envelope. These settings were used because the $t < T_A$ region contains almost no signal, and in the region where $t > T_P$, the contributions of multiple reflections in the cancellous bone might not be negligible.

In the least squares process, the fast and slow waves are estimated alternately and recurrently. The objective functions used for fitting of the fast and slow waves are expressed by the following formula:

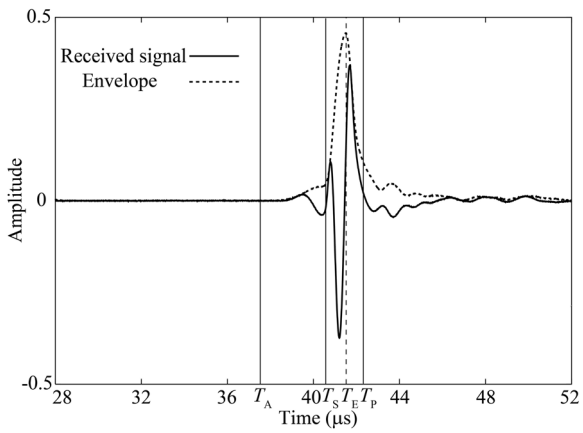

FIG. 6. Fitting region used in the least squares method. T_E is the peak time of the envelope, and T_S is the rise time of the slow wave calculated using the FDI imaging method. $T_A = T_E - 4\,\mu$s, and $T_P = T_E + 0.8\,\mu$s.

$$s_o(t) = \begin{cases} s_R(t) - s_{E2}(t) & (i = 1), \\ s_R(t) - s_{E1}(t) & (i = 2), \end{cases} \tag{23}$$

where $s_R(t)$ is the received signal, and $s_{E1}(t)$ and $s_{E2}(t)$ are the fast and slow waves that were estimated in the previous least mean squares process, respectively. At the beginning of the estimation process, $s_{E1}(t) = s_{E2}(t) = 0$.

First, the slow wave is estimated using the least mean squares method, where the fitting region is set as $T_S \le t \le T_P$, i.e., $T_1 = T_S$ and $T_2 = T_P$ in Eq. (22). To estimate the fast wave, the method is applied to a region where the contribution of the slow wave is negligible. The fitting region for the fast wave is therefore set as $T_A \le t \le T_S$. After estimation of the fast wave, the slow wave is estimated for a fitting region of $T_A \le t \le T_P$. The initial estimation of the slow wave uses the posterior fitting region of $T_S \le t \le T_P$, because the fast wave has not been eliminated from the objective function for slow wave fitting. The number of iteration steps at the fitting of the fast and slow waves ranged from 1 to 5.

III. RESULTS

Figure 7 shows the fast and slow waves in the simulation study that were estimated using the proposed decomposition method. Figure 8 shows the estimated fast and slow waves in the experimental study. In both cases, the summation of the estimated fast and slow waves strongly agreed with the received signal. Figure 9 shows the residual intensity normalized with respect to the intensity of the received signal over the whole fitting region of $T_A \le t \le T_P$, which has a width of 4.8 μs. The proposed method succeeded to characterize of the fast and slow waves accurately, where the residual intensity normalized with respect to the received signal intensity was less than -20 dB in the experimental study. In the simulation study, the residual intensity was less than -20 dB when the specimen thickness was from 3 to 8 mm. In both the simulation and experimental studies, the number of iteration steps had only a slight effect on the results. These results demonstrate the high performance and robustness of the proposed method in the estimation of fast and slow waves. The calculation time required to estimate

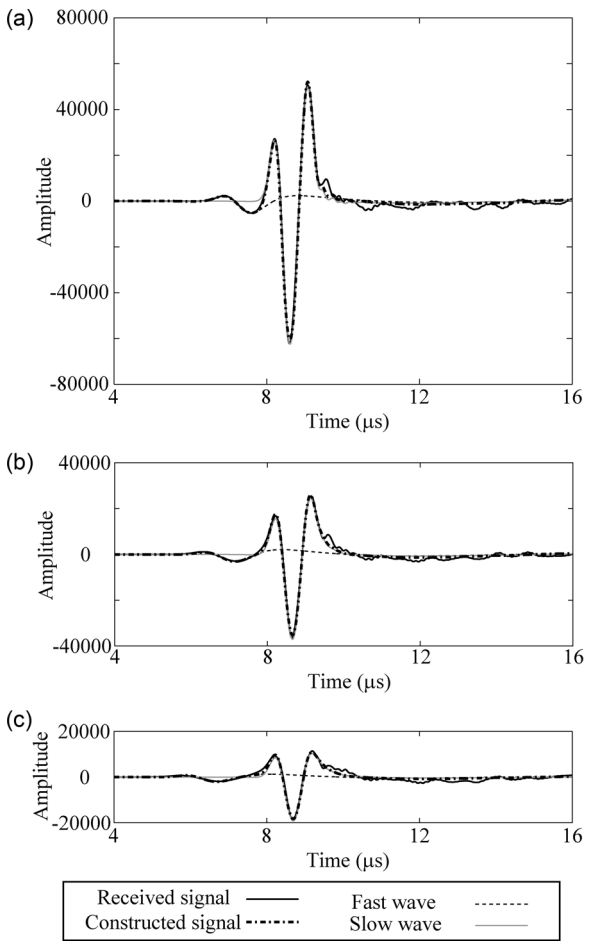

FIG. 7. Fast and slow waves estimated by the proposed decomposition method for specimen thicknesses of (a) 4 mm, (b) 6 mm, and (c) 8 mm in the simulation study. Each constructed signal represents the summation of the estimated fast and slow waves.

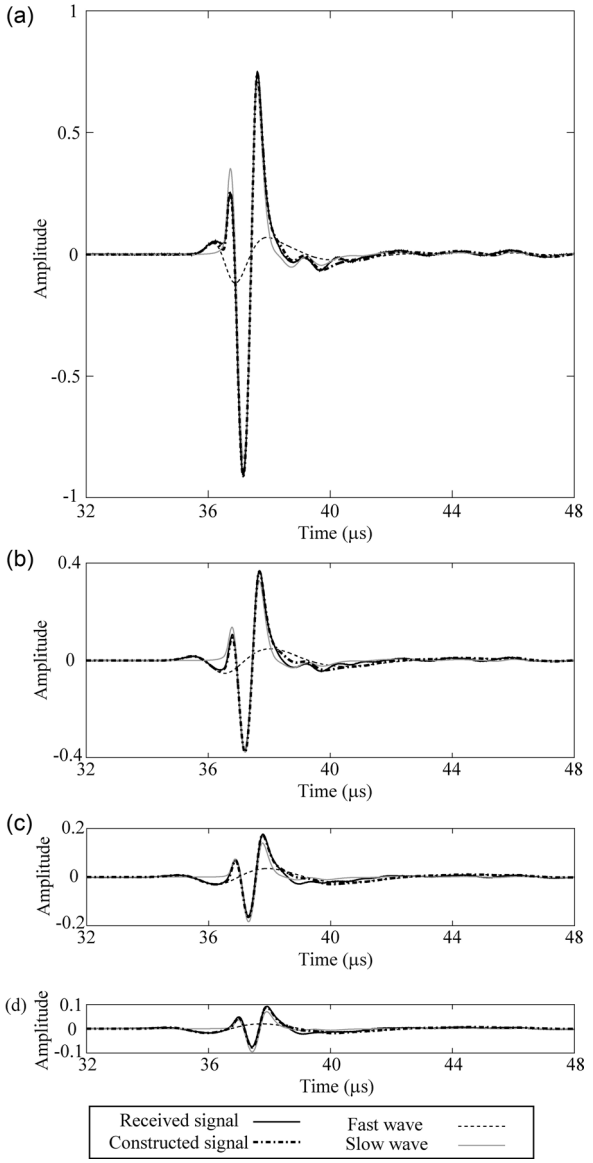

FIG. 8. Fast and slow waves estimated by the proposed decomposition method for specimen thicknesses of (a) 6 mm, (b) 9 mm, (c) 12 mm, and (d) 15 mm in the experimental study. Each constructed signal represents the summation of the estimated fast and slow waves.

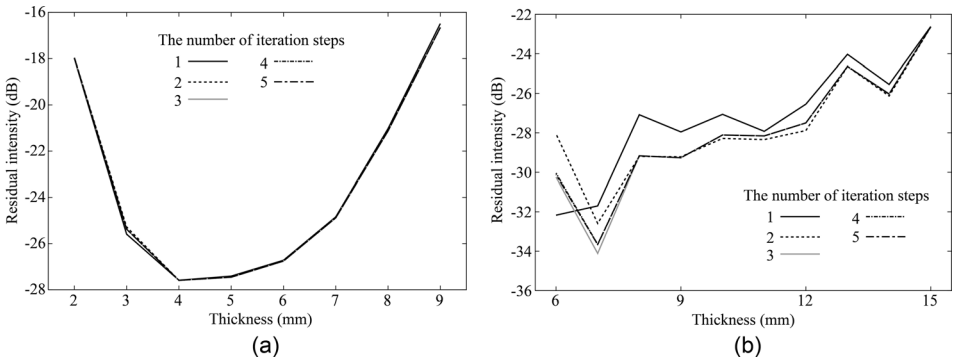

FIG. 9. Residual intensity in (a) the simulation study and (b) the experimental study when normalized with respect to the intensity of the received signal over the entire fitting region, which has a width of 4.8 μs. The number of iteration steps at the fitting of fast and slow waves is from 1 to 5.

the fast and slow waves for a single received signal was 5 s using a laptop personal computer (PC) with a single central processing unit (CPU), where the number of iteration steps was 3.

IV. DISCUSSION

Figure 9 shows that a single estimation process was sufficient for accurate characterization of the fast and slow waves, and that the number of iteration steps had only a small effect on the characterization performance. The high performance and robustness of the proposed method may originate from the accurate estimation of the rise time of the slow wave, T_S, using the FDI imaging method. Because the fitting region for the fast wave is $t < T_S$, the accurate estimation of T_S provides an appropriate fitting region for the fast wave that is wide and is little affected by the estimated slow wave. Therefore, the number of iteration steps may have a small effect on the estimation of the fast wave using the proposed method, as indicated by the results shown in Fig. 9.

In most cases, the least mean squares process used all 111 candidates, especially for the slow wave fitting process. In the simulation study, the average numbers of candidates used by the process were 72.5 and 111 for the fast and slow waves, respectively. In the experimental study, 89.2 and 102.1 candidates were used for the fast and slow waves, respectively. The proposed method used the candidates with peak intensities that were higher than 1/100 of the maximum peak intensity, and a more severe constraint will suppress the computational load, although it would be at the cost of some robustness.

The proposed decomposition method estimated the specimen thickness, the signal amplitude and the phase rotation for each wave. We calculated the signal amplitudes A_i' and the slopes of attenuation (broadband ultrasonic attenuation parameters) β_i' from the true specimen thickness and using the parameters estimated by the proposed method, as shown in Fig. 10. In the experimental study, the signal amplitude of the fast wave was higher than 1 under all specimen thickness conditions. This is inconsistent with Eq. (5), because the signal amplitude should be less than 1. This result indicates that the linear-with-frequency attenuation model may be inappropriate for the fast wave transfer model at least. The frequency components of the fast wave that were estimated by the proposed method may agree with those of the true fast wave in the high signal-to-noise ratio range, as shown in Fig. 11. Because the true signal amplitude should be less than 1, the attenuation coefficient of the fast wave $\alpha_1(f)$ may be written using the following formula:

$$\alpha_1(f) = \beta_1 f^y \quad (y > 1). \tag{24}$$

The use of an attenuation model described by a power law, i.e., the model given by Eq. (24), should improve the estimation accuracy for characterization of the fast and slow waves; however, this also causes a large increase in the computational load. Because the residual intensity normalized with respect to the received signal was less than -20 dB, the linear-with-frequency attenuation model may be sufficient for the proposed decomposition method.

Figure 12 shows the phase rotation values θ_i for the fast and slow waves that were estimated by the proposed method

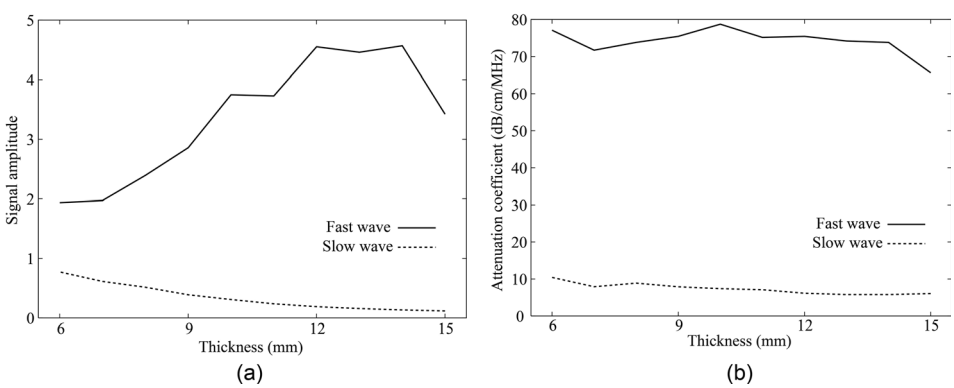

FIG. 10. (a) Signal amplitudes and (b) slopes of attenuation (broadband ultrasonic attenuation parameters) for the fast and slow waves in the experimental study estimated using the proposed decomposition method with a linear-with-frequency attenuation model.

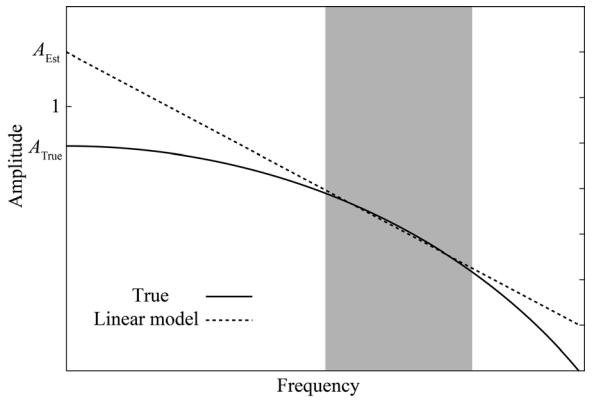

FIG. 11. Schema of the signal amplitude of a frequency component, where the longitudinal axis uses a logarithmic scale. A_{True} and A_{Est} are the true signal amplitude and the estimated amplitude, respectively, and were obtained using the proposed method with the linear-with-frequency attenuation model. The gray region denotes the frequency components with high signal-to-noise ratios.

in the experimental study. The phase rotation of the slow wave seemed to be constant. In contrast, the phase rotation of the fast wave varied, and its differential seemed to be related to the differential of the specimen thickness. This result can be explained by introducing the hypothesis that wave transfer in a cancellous bone causes a physical phenomenon, e.g., the uneven wavefront, and the phase rotation originates from this phenomenon. Because the slow wave mainly transfers in the bone marrow, which is a liquid material, this physical phenomenon may not occur and the phase rotation may in fact be independent of the specimen thickness. The constant phase rotation may originate at the moments of transmission and reception of the ultrasound wave, where it might be caused by the waveform change that originated from the uneven wavefront. In contrast, the fast wave mainly transfers in the bone structure. Therefore, the physical phenomenon may occur at the point of transfer in the bone, and the cumulative effect of this phenomenon may cause the phase rotation that depends on the specimen thickness. This consideration may validate the use of the phase rotation parameter in the transfer function.

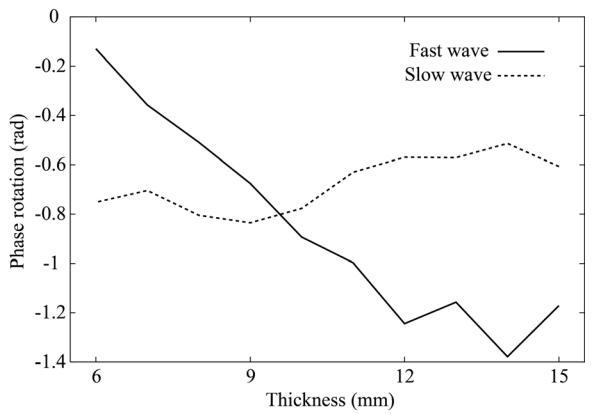

FIG. 12. Phase rotation values θ_i for the fast and slow waves estimated using the proposed method in the experimental study.

V. CONCLUSION

In this study, we proposed a novel fast decomposition method based on the FDI imaging method, where the FDI imaging method enables accurate determination of the border between the fast and slow waves. In addition, we proposed a modified wave transfer function using a phase rotation parameter that may compensate for the waveform change caused by the uneven wavefront. The proposed method provided accurate characterization of the fast and slow waves, where the residual intensity normalized with respect to the received signal intensity was found to be less than −20 dB in an experimental study using bone specimens with thicknesses ranging from 6 to 15 mm. In the simulation study, the residual intensity was less than −20 dB when the specimen thickness was from 3 to 8 mm. The characterization of the fast and slow waves for a single received signal takes only 5 s using a laptop PC with a single CPU. We believe that this method has great potential to provide good indicators of osteoporosis accurately and rapidly.

ACKNOWLEDGMENTS

This work was partly supported by the Innovative Techno-Hub for Integrated Medical Bio-imaging Project of the Special Coordination Funds for Promoting Science and Technology from the Ministry of Education, Culture, Sports, Science and Technology (MEXT), Japan, and by MEXT/JSPS KAKENHI through Grant Nos. 25870345 and 25871038.

Anderson, C. C., Bauer, A. Q., Holland, M. R., Pakula, M., Laugier, P., Bretthorst, G. L., and Miller, J. G. (**2010**). "Inverse problems in cancellous bone: Estimation of the ultrasonic properties of fast and slow waves using Bayesian probability theory," J. Acoust. Soc. Am. **128**, 2940–2948.

Anderson, C. C., Marutyan, K. R., Holland, M. R., Wear, K. A., and Miller, J. G. (**2008**). "Interference between wave modes may contribute to the apparent negative dispersion observed in cancellous bone," J. Acoust. Soc. Am. **124**, 1781–1789.

Barkmann, R., Laugier, P., Moser, U., Dencks, S., Klausner, M., Padilla, F., Haïat, G., and Glüer, C. C. (**2008a**). "A device for *in vivo* measurements of quantitative ultrasound variables at the human proximal femur," IEEE Trans. Ultrason. Ferroelectr. Freq. Control **55**, 1197–1204.

Barkmann, R., Laugier, P., Moser, U., Dencks, S., Klausner, M., Padilla, F., Haïat, G., and Glüer, C. C. (**2008b**). "*In vivo* measurements of ultrasound transmission through the human proximal femur," Ultrasound Med. Biol. **34**, 1186–1190.

Blake, G. M., and Fogelman, I. (**2007**). "Role of dual-energy X-ray absorptiometry in the diagnosis and treatment of osteoporosis," J. Clin. Densitometry **10**, 102–110.

Bouxsein, M. L., Courtney, A. C., and Haynes, W. C. (**1995**). "Ultrasound and densitometry of the calcaneus correlate with the failure loads of cadaveric femurs," Calcif. Tissue Int. **56**, 99–103.

Capon, J. (**1969**). "High resolution frequency-wavenumber spectrum analysis," Proc. IEEE **57**, 1408–1418.

Cardoso, L., Teboul, F., Sedel, L., Oddou, C., and Meunier, A. (**2003**). "*In vitro* acoustic waves propagation in human and bovine cancellous bone," J. Bone Miner. Res. **18**, 1803–1812.

Dencks, S., and Schmitz, G. (**2013**). "Estimation of multipath transmission parameters for quantitative ultrasound measurements of bone," IEEE Trans. Ultrason. Ferroelectr. Freq. Control **60**, 1884–1895.

Fellah, Z. E., Chapelon, J. Y., Berger, S., Lauriks, W., and Depollier, C. (**2004**). "Ultrasonic wave propagation in human cancellous bone: Application of Biot's theory," J. Acoust. Soc. Am. **116**, 61–73.

Genant, H. K., and Jiang, Y. (**2006**). "Advanced imaging assessment of bone quality," Ann. N.Y. Acad. Sci. **1068**, 410–428.

Haïat, G., Padilla, F., Peyrin, F., and Laugier, P. (**2007**). "Variation of ultrasonic parameters with microstructure and material properties of trabecular bone: A 3D model simulation," J. Bone Miner. Res. **22**, 665–674.

Haïat, G., Padilla, F., Svrcekova, M., Chevalier, Y., Pahr, D., Peyrin, F., Laugier, P., and Zysset, P. (**2009**). "Relationship between ultrasonic parameters and apparent trabecular bone elastic modulus: A numerical approach," J. Biomech. **42**, 2033–2039.

Han, S., Medige, J., Davis, J., Fishkin, Z., Mihalko, W., and Ziv, I. (**1997**). "Ultrasound velocity and broadband attenuation as predictors of loadbearing capacities of human calcanei," Calcif. Tissue Int. **60**, 21–25.

Hoffman, J. J., Nelson, A. M., Holland, M. R., and Miller, J. G. (**2012**). "Cancellous bone fast and slow waves obtained with Bayesian probability theory correlate with porosity from computed tomography," J. Acoust. Soc. Am. **132**, 1830–1837.

Hosokawa, A. (**2009**). "Numerical analysis of variability in ultrasound propagation properties induced by trabecular microstructure in cancellous bone," IEEE Trans. Ultrason. Ferroelectr. Freq. Control **56**, 738–747.

Hosokawa, A., and Otani, T. (**1997**). "Ultrasonic wave propagation in bovine cancellous bone," J. Acoust. Soc. Am. **101**, 558–562.

Hosokawa, A., and Otani, T. (**1998**). "Acoustic anisotropy in bovine cancellous bone," J. Acoust. Soc. Am. **103**, 2718–2722.

Hughes, E. R., Leighton, T. G., Petley, G. W., and White, P. R. (**1999**). "Ultrasonic propagation in cancellous bone: A new stratified model," Ultrasound Med. Biol. **25**, 811–821.

Hughes, E. R., Leighton, T. G., White, P. R., and Petley, G. W. (**2007**). "Investigation of an anisotropic tortuosity in a Biot model of ultrasonic propagation in cancellous bone," J. Acoust. Soc. Am. **121**, 568–574.

Kaczmarek, M., Kubik, J., and Pakula, M. (**2002**). "Short ultrasonic waves in cancellous bone," Ultrasonics **40**, 95–100.

Langton, C. M., Palmer, S. B., and Porter, R. W. (**1984**). "The measurement of broadband ultrasonic attenuation in cancellous bone," Eng. Med. **13**, 89–91.

Laugier, P. (**2008**). "Instrumentation for *in vivo* ultrasonic characterization of bone strength," IEEE Trans. Ultrason. Ferroelectr. Freq. Control **55**, 1179–1196.

Lochmüller, E. M., Eckstein, F., Zeller, J. B., Steldinger, R., and Putz, R. (**1999**). "Comparison of quantitative ultrasound in the human calcaneus with mechanical failure loads of the hip and spine," Ultrasound Obstet. Gynecol. **14**, 125–133.

Marutyan, K. R., Bretthorst, G. L., and Miller, J. G. (**2007**). "Bayesian estimation of the underlying bone properties from mixed fast and slow mode ultrasonic signals," J. Acoust. Soc. Am. **121**, EL8–EL15.

Marutyan, K. R., Holland, M. R., and Miller, J. G. (**2006**). "Anomalous negative dispersion in bone can result from the interference of fast and slow waves," J. Acoust. Soc. Am. **120**, EL55–EL61.

Mizuno, K., Matsukawa, M., Otani, T., Laugier, P., and Padilla, F. (**2009**). "Propagation of two longitudinal waves in human cancellous bone: An *in vitro* study," J. Acoust. Soc. Am. **125**, 3460–3466.

Mizuno, K., Matsukawa, M., Otani, T., Takada, M., Mano, I., and Tsujimoto, T. (**2008**). "Effects of structural anisotropy of cancellous bone on speed of ultrasonic fast waves in the bovine femur," IEEE Trans. Ultrason. Ferroelectr. Freq. Control **55**, 1480–1487.

Nagatani, Y., Mizuno, K., Saeki, T., Matsukawa, M., Sakaguchi, T., and Hosoi, H. (**2008**). "Numerical and experimental study on the wave attenuation in bone—FDTD simulation of ultrasound propagation in cancellous bone," Ultrasonics **48**, 607–612.

Nelson, A. M., Hoffman, J. J., Anderson, C. C., Holland, M. R., Nagatani, Y., Mizuno, K., Matsukawa, M., and Miller, J. G. (**2011**). "Determining attenuation properties of interfering fast and slow ultrasonic waves in cancellous bone," J. Acoust. Soc. Am. **130**, 2233–2240.

Njeh, C. F., Hans, D., Fuerst, T., Glüer, C. C., and Genant, H. K. (**1999**). *Quantitative Ultrasound: Assessment of Osteoporosis and Bone Status* (Martin Dunitz, London), pp. 1–432.

Njeh, C. F., Kuo, C. W., Langton, M. M., Atrah, H. I., and Boivin, C. M. (**1997**). "Prediction of human femoral bone strength using ultrasound velocity and BMD: An *in vitro* study," Osteoporosis Int. **7**, 471–477.

Taki, H., Taki, K., Sakamoto, T., Yamakawa, M., Shiina, T., Kudo, M., and Sato, T. (**2012**). "High range resolution ultrasonographic vascular imaging using frequency domain interferometry with the Capon method," IEEE Trans. Med. Imaging **31**, 417–429.

Waters, K. R., Mobley, J., and Miller, J. G. (**2005**). "Causality-imposed (Kramers-Kronig) relationships between attenuation and dispersion," IEEE Trans. Ultrason. Ferroelectr. Freq. Control **52**, 822–833.

Wear, K. A. (**2013**). "Estimation of fast and slow wave properties in cancellous bone using Prony's method and curve fitting," J. Acoust. Soc. Am. **133**, 2490–2501.

Wear, K. A. (**2014**). "Time-domain separation of interfering waves in cancellous bone using band limited deconvolution: Simulation and phantom study," J. Acoust. Soc. Am. **135**, 2102–2112.